Dynamics and thermodynamics of systems with long-range dipole-type interactions

Boris Atenas and Sergio Curilef*
Departamento de Física, Universidad Católica del Norte, Avenida Angamos 0610, Antofagasta, Chile
(Received 22 September 2015; revised manuscript received 6 May 2016; published 8 February 2017; corrected 29 March 2017)

A Hamiltonian mean field model, where the potential is inspired by dipole-dipole interactions, is proposed to characterize the behavior of systems with long-range interactions. The dynamics of the system remains in quasistationary states before arriving at equilibrium. The equilibrium is analytically derived from the canonical ensemble and coincides with that obtained from molecular dynamics simulations (microcanonical ensemble) at only long time scales. The dynamics of the system is characterized by the behavior of the mean value of the kinetic energy. The significance of the results, compared to others in the recent literature, is that two plateaus sequentially emerge in the evolution of the model under the special considerations of the initial conditions and systems of finite size. The first plateau decays to a different second one before the system reaches equilibrium, but the dynamics of the system is expected to have only one plateau when the thermodynamics limit is reached because the difference between them tends to disappear as N tends to infinity. Hence, the first plateau is a type of quasistationary state the lifetime of which depends on a power law of N and the second seems to be a true quasistationary state as reported in the literature. We characterize the general behavior of the model according to its dynamics and thermodynamics.

DOI: 10.1103/PhysRevE.95.022110

I. INTRODUCTION

Systems with long-range interactions are very common in nature. They are observed from the atomic scale to the astronomical scale and exhibit anomalies, such as inequivalence of ensembles, negative heat capacity, ergodicity breaking, nonequilibrium phase transitions, quasistationary states, and anomalous diffusion [1–4]. These anomalies are exacerbated when special initial conditions are imposed [4]. The canonical ensemble in statistical mechanics does not explain the molecular dynamics on a short time scale, although it proves to be correct on a larger canonical and microcanonical time scales, where the phase diagrams overlap at equilibrium only.

An intriguing model used to characterize systems with long-range interactions is the Hamiltonian mean field (HMF) model [4,5], in which properties become axiomatic and pertinent. This characterization also appears to be shared by other systems of this type. The existence of quasistationary states (QSS) before reaching equilibrium constitutes a fingerprint of systems with long-range interactions. The behavior of the kinetic energy and other thermodynamic observables are partly used to characterize the QSS in physical models and systems [5,6].

Lynden-Bell statistics [6] approaches the general behavior of long-range interacting systems such as the HMF model [1]. The theory proposes that systems with long-range interactions can be trapped in QSS, unlike systems with short-range interactions, which are going directly to equilibrium. Such a description is based on Vlasov dynamics, which preserves the hypervolume of phase-space density levels, and the distribution functions are the solutions of the Vlasov equation. The construction of Lynden-Bell statistics is similar to the Boltzmann theory, but instead of working with particles, a type of Fermi-Dirac distribution is used for the phase-space density levels, which includes the single-particle energy and the phase-space density of the initial distribution. Additionally, Lynden-Bell statistics requires the existence of ergodicity and mixing properties, similar to the usual statistical mechanics, which are not valid for systems with long-range interactions where those properties are not upheld.

The primary motivation of this study is to help envision potential future applications in nanoscience and nanotechnology involving systems of rotors mounted on surfaces or inside solids. Most molecular rotors have been studied in solution. After all, the rotor molecules synthesis and their basic characteristics such as rotational barriers are nearly always established in solution before mounting them on surfaces or examining them inside solids [7]. Besides, to many authors, the investigation of molecular rotors freely floating in a solution is in itself a fascinating topic [7,8]. In this regard, families of HMF models may have a favorable outlook. Nevertheless, a variety of molecular systems that can exhibit controlled rotational motion [9] have been created. In the development of such systems, the key step is the addition of communication between molecules in a network. Therefore, the total energy of the rotor network, for the observed synchronized rotation mechanism, is analyzed through a model that is described by energy terms composed of the internal rotational kinetic energy, the dipole energy, the external field energy, the structural energy including the dispersion interactions in the network, and the thermal energy corresponding to a specific substrate temperature [9]. We approach the model by taking into account two terms in a Hamiltonian, namely, the classical rotational energy and dipole potential in the mean field approximation.

Previous studies discuss some interesting systems related to charges, spins, rotors, and dipoles, such as charged particles [10] and noninteracting dipoles [11] in an external magnetic field, long-range interactions in a type of Ising model, and other generalized models [12,13]. The present work focuses on rotor-rotor interactions that depend on the orientation of dipoles in the mean field approximation. The main aim is to characterize the dynamics and thermodynamics of systems with long-range interactions based on the dipole-dipole potential energy [7].

*scurilef@ucn.cl

For several years, the Ising model has been considered the most relevant tool for studying magnetic properties and the statistical behavior of many-body systems. Great efforts have been made to propose several variations of the Ising model, especially for the theoretical and numerical modeling of systems with long-range interactions [1,3], which encompasses the family of HMF models [4]. We propose a model based on the dipole-dipole interaction to search for new properties that are general to these types of models. We use the canonical ensemble to calculate the free energy, magnetization, and internal energy at the equilibrium. Using numerical simulation we characterize the mean kinetic energy, distributions, caloric curve, and the diffusion law through the mean square of displacement.

The paper is organized as follows. In Sec. II, we introduce an HMF model (that we call d-HMF) to study systems with long-range interactions. In Sec. III, we analytically solve the statistics of the system in the canonical ensemble and show the behavior of the system in the microcanonical ensemble through molecular dynamics simulations. We also introduce some diffusion properties of the system. Finally, Sec. IV summarizes the results and presents the conclusions.

II. THE MODEL

For theoretical and numerical modeling of systems with long-range interactions, we consider a system of N identical, coupled, dipole-type particles with a mass equal to 1. The dynamics evolves in a periodic cell described by a one-dimensional, dipole-type, HMF model (d-HMF) given by

$$H = \sum_{i=1}^{N} \frac{p_i^2}{2} + \frac{\epsilon}{2N} \sum_{i \neq j}^{N} [\cos(\theta_i - \theta_j) - 3\cos\theta_i \cos\theta_j - \Delta_{i,j}], \quad (1)$$

where the variable p_i represents the momentum of the particle i, and θ_i represents its corresponding angle of orientation (integer $i \in [1,N]$ for the system size N). The parameters ϵ and $\Delta_{i,j}$ denote the coupling and initial conditions, respectively. The parameter $\Delta_{i,j}$ suitably establishes the zero of the potential energy as

$$\Delta_{i,j} = \cos(\theta_{0i} - \theta_{0j}) - 3\cos\theta_{0i}\cos\theta_{0j}, \quad (2)$$

where the set of angles $\{\theta_{0k}\}$ denotes the initial orientations of the particles. The interaction coupling is rescaled by the number of particles to make the potential thermodynamically extensive [12–14]. The system is ferromagnetic if the coupling ϵ is positive and antiferromagnetic if it is negative. The equilibrium state can be exactly derived but the QSS are not standard and cannot be exactly obtained from the theory. Numerical methods have become an acceptable tool for the study and characterization of these anomalies. Following a previous line of research, we describe the behavior of a dipole in a uniform magnetic field [11]. However, the current discussion shows some details related to these interactions. The spin vector related to each particle is given by $\vec{m}_i = (\cos\theta_i, \sin\theta_i)$. Therefore, we can introduce the total spin vector

$$\vec{M} = \frac{1}{N} \sum_{i=1}^{N} \vec{m}_i = (M_x, M_y) = M \exp(i\phi), \quad (3)$$

where (M_x, M_y) and M are the components and the modulus of the vector $\vec{M}$, respectively, and ϕ denotes the phase of the order parameter. The equation of motion is

$$\dot{p}_i = -\frac{\epsilon}{2}(2M_x \sin\theta_i + M_y \cos\theta_i) \quad (4)$$

and the potential can be written as

$$V = -N\frac{\epsilon}{2}\left(2M_x^2 - M_y^2 + \Delta\right), \quad (5)$$

where $\Delta = \sum_{i,j} \Delta'_{i,j}$ with $\Delta'_{i,j} = \Delta_{i,j}/N^2$ and defines the zero of the energy.

III. DISCUSSION

In this section, we discuss analytical and numerical results that characterize the present model. In Sec. III A, an analytical approach in the canonical ensemble that corresponds to the equilibrium of the system is obtained. In Sec. III C, numerical simulations in the microcanonical ensemble are carried out through molecular dynamics. The evolution of the system is characterized by two time intervals of QSS. In Sec. III D, the obtained dynamical intervals are typified by anomalous diffusion.

A. The equilibrium

In the canonical ensemble, the partition function is

$$Z(\beta,N) = \int \mathrm{d}^N p_i \, \mathrm{d}^N \theta_i e^{-\beta H} = Z_K(\beta,N) Z_V(\beta,N), \quad (6)$$

where $Z_K(\beta,N)$ is the kinetic part of the integral and $Z_V(\beta,N)$ is the interacting part. Therefore, if $\{\theta_{0,i} = 0\}$ for all i,

$$Z_K(\beta,N) = \int \mathrm{d}^N p_i \exp\left(-\frac{\beta}{2}\sum_i p_i^2\right) = \left(\frac{2\pi}{\beta}\right)^{N/2}. \quad (7)$$

Considering both the real and complex Hubbard-Stratonovich transformations [16,17], we obtain

$$Z_V(\beta,N) = \sqrt{\frac{\beta\epsilon N}{\pi}} e^{\frac{\Delta}{2}\beta\epsilon N} \int_{-\infty}^{\infty} \mathrm{d}x \, e^{-\beta\epsilon N x^2} \mathrm{I}_0(2\beta\epsilon x)^N, \quad (8)$$

where $\mathrm{I}_k(y)$ is the kth-order modified Bessel function. This integral can be evaluated using the saddle point method in the thermodynamic limit for $N \to \infty$. The free energy per particle φ is given by

$$\varphi(\beta,N) = \frac{1}{2}\ln\frac{\beta}{2\pi} - \frac{\Delta}{2}\epsilon\beta + \inf_{x \geqslant 0}[-\beta\epsilon x^2 + \ln \mathrm{I}_0(2\beta\epsilon x)]. \quad (9)$$

The solution of the extremal is obtained by

$$x = \frac{\mathrm{I}_1(2\beta\epsilon x)}{\mathrm{I}_0(2\beta\epsilon x)}. \quad (10)$$

The procedure is specific to this problem because it includes the complex Hubbard-Stratonovich transformation [16,17], although it is also partly analogous to the HMF model. The critical temperature is $T_c = 1$, which is twice that obtained for the HMF model. The clustered phase is found for $T < T_c$, and the homogeneous phase occurs for $T > T_c$. If $\epsilon < 0$, then the equation has a trivial solution, $x = 0$. In contrast, if $\epsilon > 0$, then the equation has a set of values for x and β, which define the

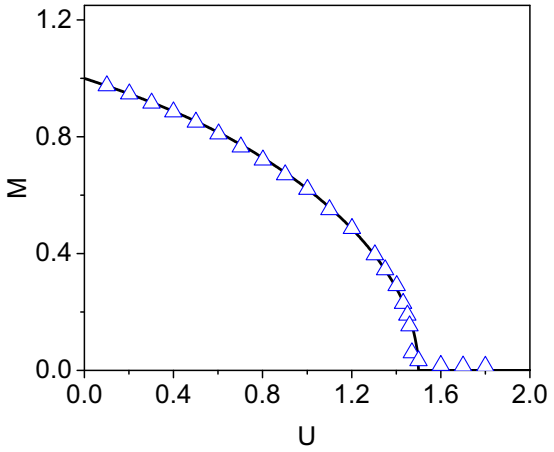

FIG. 1. Equilibrium magnetization as a function of internal energy U. Simulation data (triangles) and the analytical solution (solid line) from Eq. (11) are shown. The size of the simulated systems is $N = 4000$ and the averages are made for 100 samples.

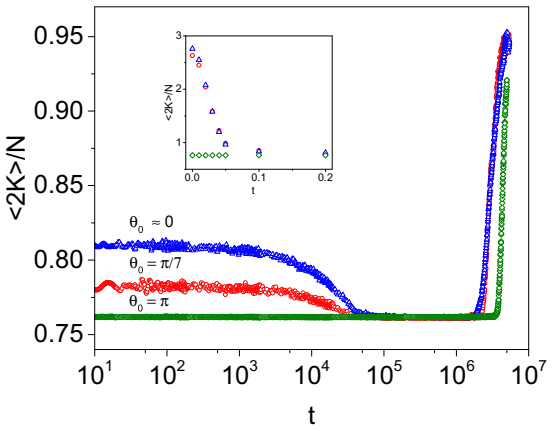

FIG. 2. The evolution of the average over 100 samples of the kinetic energy with $N = 25\,000$ as a function of the time for 100 samples. The evolution from three different initial conditions of $\theta_0 = 10^{-4}, \pi/7$, and π are presented. In the homogeneous case ($\theta_0 = \pi$), the behavior is similar to the HMF model. In the extremely inhomogeneous case, $\theta_0 \approx 0$, the anomaly is highest and we use this case to characterize the two QSS. The inset shows the first evolution, which is known as violent relaxation on a linear scale.

solution of the problem. Finally, the internal energy per particle is obtained as a function of the temperature and magnetization:

$$U = \frac{\partial \varphi(\beta, N)}{\partial \beta} = \frac{1}{2\beta} - \frac{\Delta}{2} - M^2, \tag{11}$$

where M is the solution of the extremal problem and corresponds to the solution that we derive from the canonical ensemble. Thus, we obtain a solution by simulating the microcanonical ensemble for several energy values. Figure 1 depicts the equilibrium magnetization M as a function of the internal energy U. Numerical data are represented by triangles. The analytical solution is depicted by the solid line obtained from the canonical ensemble given by Eq. (11). The critical point is located at $U_c = 3/2$, which is twice the value obtained for the HMF model.

B. Initial conditions

Another challenge is evaluating the kinetic energy. The behavior of this thermodynamic quantity is required to define some properties of the system. In the first stage, we can set the zero of the energy as $\Delta = -2$ according to Eq. (5). As shown in Eq. (11), the parameter Δ produces just a linear shift in the energy.

In the dynamics of the model, it is important to observe where the kinetic energy is constant, which is relevant for determining the general behavior of other thermodynamic observables.

To discuss the evolution of thermodynamical properties of the system, we carry out molecular dynamics simulation using a symplectic integrator [15] and water bag initial conditions (WBIC). For the latter, consider particles confined in a bounded domain in phase space that initially displays a uniform distribution. Thus, the general definition of the WBIC is related to the probability distribution function $f(\theta, p)$ as

$$f(x,p)\,\mathrm{d}\theta\,\mathrm{d}p = \frac{\mathrm{d}\theta\,\mathrm{d}p}{4\,\theta_0\,p_0}, \tag{12}$$

where $-p_0 \leqslant p \leqslant p_0$ and $-\theta_0 \leqslant \theta \leqslant \theta_0$, which is properly normalized in the entire space. If $\theta_0 = \pi$ the function $f(x,p)$ may be called "homogeneous in space" and it is a stationary solution of the Vlasov equation [18,19]. In the inhomogeneous case, where $0 < \theta_0 < \pi$, the dynamics of the system is expected to evolve in a self-consistent way to satisfy the pertinent thermodynamic properties. We shall discuss the case where θ_0 is close to zero, which corresponds to the case where the dipoles are aligned in almost the same direction. We characterize the properties of the system with this kind of WBIC because the anomalous behavior is exacerbated.

Figure 2 presents the average dynamics of the system by the evolution of $2\langle K\rangle/N$ in 100 samples with $N = 25\,000$ particles. The difference among curves comes from the three different sets of initial conditions considered. We take the WBIC given by Eq. (12) with a typical value of p_0 and three different values of θ_0, which typically correspond to the extremely inhomogeneous case ($\theta_0 \approx 0$), an intermediate inhomogeneous case ($\theta_0 = \pi/7$), and the completely homogeneous cases ($\theta_0 = \pi$). In the inset of Fig. 2, the first evolution is known as violent relaxation, which is clearly shown when WBIC are inhomogeneous. For the homogeneous case the quantity $2\langle K\rangle/N = 0.76$ coincides with its numerical value for the second QSS. The dynamics of the HMF model does not present evident differences if variations on the WBIC are considered, but d-HMF shows two different plateaus when the WBIC depart from the homogeneous case. Therefore, the results, shown in Fig. 2, emphasize the relevance of the initial conditions in the dynamics of the problem. The appearance of two plateaus before reaching the equilibrium is due to considering the inhomogeneous WBIC.

C. Quasistationary states

This subsection discusses some of the thermodynamic properties obtained from the simulations that are related to

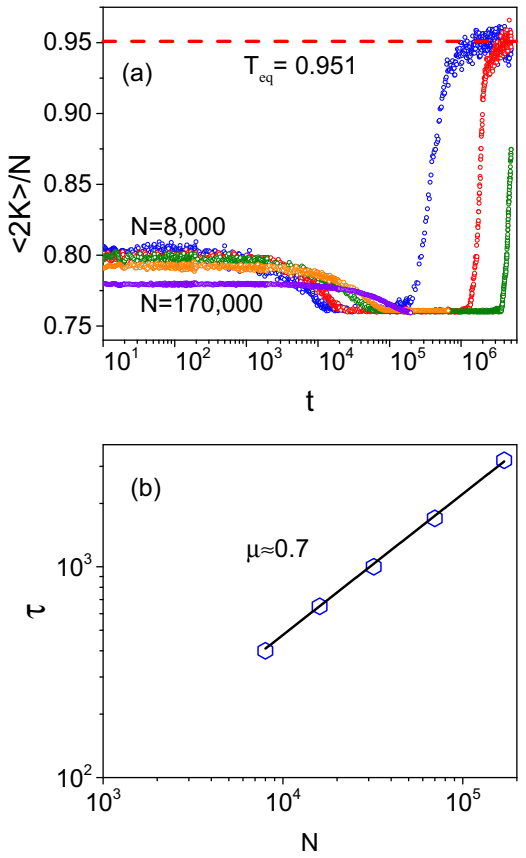

FIG. 3. The dependence on system size N of twice the mean kinetic energy is illustrated. The quantity $2\langle K\rangle/N$ is depicted as a function of the time. (a) Several sizes of the systems are considered. The limiting cases are $N = 8000$ and 170 000. Intermediate cases correspond to $N =$ 16 000, 32 000, and 70 000. (b) The relaxation time τ, of the first QSS that goes to the second QSS as a function of $1/N$ in log-log scale. These results are used to obtain a power law of the duration of the first QSS in terms of the system size. Thus, we expect the lifetime observed in the first QSS to behave as $\tau(N) \propto N^{0.7}$.

the effects of finite size and finite time where QSS have been observed.

Figure 3(a) shows the time evolution of $2\langle K\rangle/N$ is reported for several sizes of the system, that is, $N =$ 8000, 16 000, 32 000, 70 000, and 170 000. The limiting cases are indicated in the figure; these are $N = 8000$ and 170 000. The quantity $2\langle K\rangle/N$ shows that two plateaus with values and durations clearly depend on N. If N increases, the plateau value decreases as the duration increases. States defined by these plateaus known as the QSS are notoriously lower than the canonical temperature. WBIC stimulate the time that the systems remain in states of nonequilibrium, which are the QSS in this case. They need times that increase with N to transit from the first QSS to the second QSS, and finally to relax to the canonical equilibrium. The averages represented in Fig. 3(a) are taken for 100 samples at $N = 8000$ and for 32 samples at $N =$ 16 000, 32 000, 70 000, and 170 000.

As mentioned, the system is sensitive to the WBIC, which is shown in Fig. 3(a). In addition, these results evoke the behavior of systems that strongly depend on the system

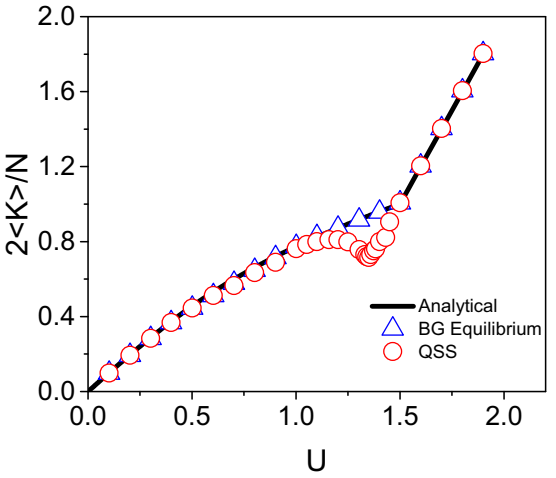

FIG. 4. $2\langle K\rangle/N$ as a function of the internal energy U. The lowest QSS (circles) and its corresponding equilibrium values (triangles) are compared to T_{eq} (line), which was obtained analytically from the canonical ensemble. The simulation requires $N = 4000$ and 100 samples.

size. The properties slowly reach the thermodynamic limit and the results seem to indicate that the difference between the two plateaus tends to disappear as $N \to \infty$. Hence, the dynamics of the system is expected to have only one plateau when the thermodynamics limit is reached. Thus, the two plateaus represent one peculiar effect induced by applying the inhomogeneous WBIC and by considering finite system size.

For simulation with $N = 32\,000$ and greater, it is not possible to observe when the mean kinetic energy reaches equilibrium in the time interval that we have used for the molecular dynamics simulation, because of the computational limitations. Hence, a detailed characterization of the duration of the second QSS as a function of system size N is a good challenge for future works. However, the behavior is expected to become similar to the QSS observed for the HMF model. Nevertheless, if we focus our attention on the first plateau, which encompasses the duration of the first QSS of $\tau(N)$, the value depends on N according to a power law given by $\tau(N) \propto N^{\mu}$. From Fig. 3(b), we obtain an approximate slope of $\mu \approx 0.7$ on a log-log scale. This slope is less than that known for the unique QSS observed in the HMF model [18]. The second QSS will be studied later, but we expect it to become similar to the unique QSS in the HMF model [18].

Additionally, we show in Fig. 2 that the value obtained from numerical data $2\langle K\rangle_{eq}/N = 0.951$ coincides with 0.1% precision with its corresponding canonical value, $T_{eq} = 0.950$.

In Fig. 4 we show the stable values of the kinetic energy as a function of U, which we identify as QSS. We chose the lowest numerical result, the second QSS, to compare to equilibrium, which we obtained from either the theoretical canonical ensemble or the numerical microcanonical simulation. There is disagreement between the molecular dynamics simulation and the canonical ensemble treatment in the interval from 1.1 to 1.5. As anticipated, there is a point where the greatest disagreement occurs at $U = 1.38$, which we used to characterize the QSS. In Fig. 4 we superpose three curves of twice the kinetic energy per particle $2\langle K\rangle/N$ as a function of internal energy U.

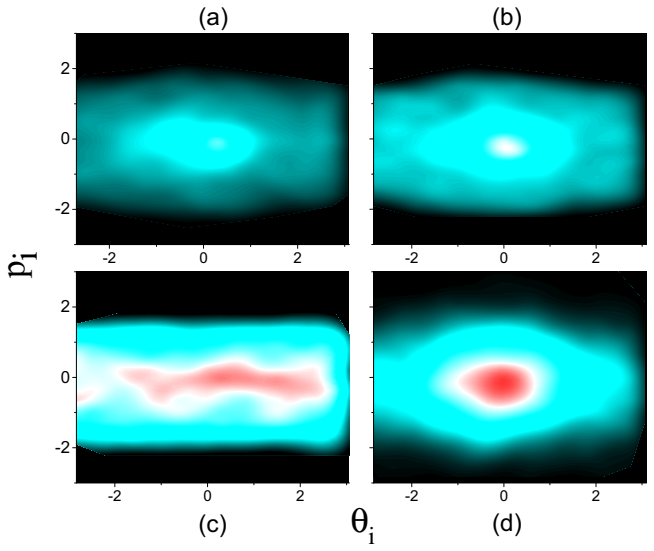

FIG. 5. Snapshots of the distribution function for the HMF model with dipole-dipole interactions into phase space. (a) For $t = 20$, the distribution weakly deviates from WBIC. (b) For $t = 200$, the system is in the first time interval of QSS. (c) For $t = 6 \times 10^5$, the system is in the second time interval of QSS. (d) For $t = 5 \times 10^6$, the system reaches equilibrium, and ellipses characterize the trajectories into phase space.

Triangles denote equilibrium data from the numerical simulations that coincide exactly with the analytical solution from the canonical ensemble. The circles correspond to the second QSS to consider values produced by the QSS from the homogeneous WBIC. As shown in Fig. 3(a), there is a time interval where one set of values does not coincide with the other.

We observed the behavior in phase space to fully understand the dynamics of the system. We can obtain instantaneous images of the particle distribution in phase space at several states of the evolution. Figure 5 presents snapshots at different times to characterize the distribution function in phase space at $t = 20$ close to WBIC; at $t = 200$, where the first QSS occurs; at $t = 6 \times 10^5$ for the second QSS; and at $t = 5 \times 10^6$, where equilibrium occurs for an arbitrary sample of a system with $N = 8000$. At $t = 0$, the system has inhomogeneous WBIC, where $\theta_0 \approx 0$ according to Eq. (12). However, the dynamics of the system seems to move rapidly in a self-consistent way to satisfy the Vlasov equation as shown in Fig. 5(a). The distribution function, in Fig. 5(b), is extended to all phase space in an irregular form. In Fig. 5(c), the distribution function takes enough paths that it shows certain regularities, which we can see in phase space. In addition, Fig. 5(d) shows trajectories that are defined by elliptical shapes, which are represented by several colors.

D. Diffusion

We represent the diffusion of particles of the system by the variance of the angular displacement defined as

$$\sigma_\theta^2(t) = \frac{1}{N}\sum_i [\theta_i(t) - \theta_i(0)]^2. \tag{13}$$

As expected, the law $\sigma_\theta^2(t) \propto t$ is valid at equilibrium only, which means that after a long time, the variance of the angular displacement varies linearly with time. Before reaching equilibrium, the law of diffusion $\sigma_\theta^2(t) \propto t^\gamma$ (where $\gamma \neq 1$) is anomalous. Particularly, the system is called subdiffusive if $0 < \gamma < 1$ and superdiffusive if $1 < \gamma < 2$.

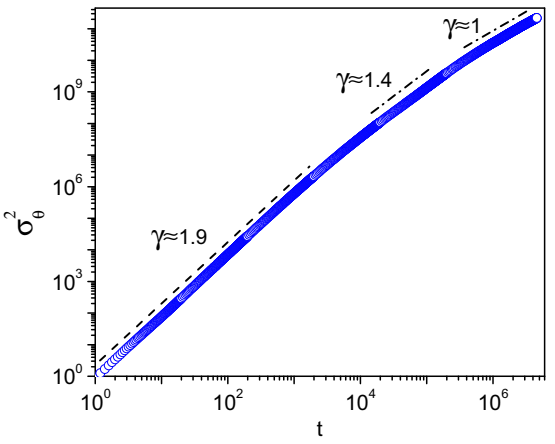

FIG. 6. The dynamics is illustrated by the evolution of the variance. Anomalous diffusion is obtained in the two time intervals that coincide with the two discussed QSS. Equilibrium is reached when $\gamma = 1$.

As predicted in previous studies [5], the anomalous diffusion is connected to QSS. We expect that two anomalous diffusion laws with two different values of γ will be related to each QSS observed in the present system.

We characterize the diffusion by using data obtained from the molecular dynamics simulation. For the same previous combination of parameters in Fig. 3, we progressively acquire states with anomalous diffusion until equilibrium is reached. Figure 6 two superdiffusive states where $\sigma_\theta^2 \propto t^\gamma$ with $\gamma > 1$, which are related to previously defined QSS. At the first QSS $\gamma \approx 1.9$; at the second QSS $\gamma \approx 1.4$; and, as expected, at equilibrium $\gamma = 1$.

IV. SUMMARY AND CONCLUDING REMARKS

The HMF model gives a good perspective for studying systems with long-range interactions. Thus, we have proposed the Hamiltonian d-HMF given by Eq. (1).

The problem was solved analytically in the canonical ensemble using the real and complex Hubbard-Stratonovich transformations to obtain the magnetization and temperature at equilibrium by using Eqs. (10) and (11). The system becomes an analytically solvable problem. Data for the equilibrium magnetization M as a function of internal energy U are represented by triangles that were obtained through molecular dynamics, which were compared to the analytical solution from Eq. (11). Both results are practically coincident in the entire range of values, except for near $T = 1.5$. The minor discrepancy is due to the finite size of the system. We also showed that the analytical calculation of the temperature matches the numerical results with 0.1% precision at equilibrium as shown in Fig. 3(a). Again, molecular dynamics data coincide exactly with the analytical result in Fig. 4, which depicts $2\langle K\rangle/N$ as a function of U. As expected, the diffusion is normal at equilibrium, where the diffusion law is a linear function of time.

It is generally accepted that two phases appear in the phase diagram, as shown in Fig. 4, which depend on the energy and thus the temperature. At low energy, a phase identified by the presence of a single cluster of particles arises by floating in a diluted homogeneous background. At high energy a homogeneous phase is recovered; the cluster disappears and the particles move (almost) freely. For a pertinent transition region below U_c, as shown in Fig. 4, the system is characterized by the microcanonical ensemble with negative specific heat and the resulting instability is extremely relevant [4] because of its strong implications on both experimental and theoretical features. It is expected that the nonequilibrium distribution related to the single cluster evolves into another nonequilibrium distribution, before reaching equilibrium. This behavior corresponds to an apparent thermodynamical inconsistency as explained by Hertel and Thirring [20], who proposed that the canonical and microcanonical ensembles are not equivalent near the transition region. We have successfully confirmed this proposal at least in an interval of time.

To describe the evolution of the proposed model, we performed molecular dynamics simulations to obtain the QSS before arriving at equilibrium. Due to the nonequilibrium states, we can define two different QSS, as shown in Fig. 3. We characterized the QSS as a constant value of the average kinetic energy. The first QSS is less than the value at equilibrium, but the second QSS value is less than the first QSS. In addition, we identified the two QSS as time intervals with anomalous diffusion, as shown in Fig. 6.

The initial conditions and the size of the systems are two relevant considerations in the present topic. Thermodynamic and dynamic properties strongly depend on the system size N, which we partially characterized for the d-HMF model. We focused on three possible initial distributions that correspond to the homogeneous WBIC and two cases of inhomogeneous WBIC. For the homogeneous WBIC, the results correspond to the standard HMF model. After the process of violent relaxation, the system remains trapped in a unique QSS before reaching the equilibrium. However, with inhomogeneous WBIC, the dynamics of the system shows two different plateaus before arriving at equilibrium, as illustrated in Fig. 2 whenever the size of the system is finite. The difference between the two plateaus tends to disappear as $N \to \infty$. Hence, the dynamics of the system is expected to have only one plateau when the thermodynamics limit is reached. The duration τ of the first QSS type depends on a power law of N [typically $\tau(N) \propto N^{0.7}$], as shown in Fig. 3. As such, it is unlikely to survive in a Vlasov picture. But, this question constitutes another challenge to study.

Due to the cost of the computational time, good topics to study in future works include description of the second QSS, ergodicity breaking, and nonequilibrium phase transitions. The results would aid in understanding the role of dipole-type interactions in nature and the behavior of systems with more than one QSS.

Additional energy terms can be considered to improve the current model, such as the external field energy, the structural energy including the dispersion interactions in the network, and the thermal energy corresponding to a specific substrate temperature [9]. This can be the challenge of upcoming proposals to obtain a more realistic Hamiltonian that allows us to compare with known results related to molecular systems.

Finally, this model appears to be consistent with other models that involve multiple QSS, such as the low-frequency variability in weather regimes [21,22], a graded autocatalysis replication domain model that undergoes a physical separation process [23], and the relaxation of turbulence in two dimensions [24]. Thus it could be a useful approach to such systems related to multiple QSS.

ACKNOWLEDGMENTS

We acknowledge partial financial support from Anillo ACT-1204 and VRIDT-UCN105/2015. We appreciate the computational assistance of A. Pluchino.

[1] Y. Levin, R. Pakter, F. B. Rizzato, T. N. Teles, and F. P. da C. Benetti, Phys. Rep. **535**, 1 (2014).
[2] Fernanda P. da C. Benetti, T. N. Teles, R. Pakter, and Y. Levin, Phys. Rev. Lett. **108**, 140601 (2012).
[3] A. Campa, T. Dauxois, and S. Ruffo, Phys. Rep. **480**, 57 (2009).
[4] M. Antoni and S. Ruffo, Phys. Rev. E **52**, 2361 (1995).
[5] A. Pluchino, V. Latora, and A. Rapisarda, Continuum Mech. Thermodyn. **16**, 245 (2004).
[6] D. Lynden-Bell, Mon. Not. R. Astron. Soc. **136**, 101 (1967).
[7] G. S. Kottas, L. I. Clarke, D. Horinek, and J. Michl, Chem. Rev. **105**, 1281 (2005).
[8] S. Erbas-Cakmak, D. A. Leigh, C. T. McTernan, and A. L. Nussbaumer, Chem. Rev. **115**, 10081 (2015).
[9] Y. Zhang, H. Kersell, R. Stefak, J. Echeverria, V. Iancu, U. G. E. Perera, Y. Li, A. Deshpande, K.-F. Braun, C. Joachim, G. Rapenne, and S.-W. Hla, Nat. Nanotechnol. **11**, 706 (2016).
[10] S. Curilef and F. Claro, Am. J. Phys. **65**, 244 (1997).
[11] B. Atenas, L. A. del Pino, and S. Curilef, Ann. Phys. **350**, 605 (2014).
[12] L. A. del Pino, P. Troncoso, and S. Curilef, Phys. Rev. B **76**, 172402 (2007).
[13] S. Curilef, Phys. Lett. A **299**, 366 (2002).
[14] M. Kac, G. Uhlenbeck, and P. C. Hemmer, J. Math. Phys. **4**, 216 (1963).
[15] H. Yoshida, Phys. Lett. A **150**, 262 (1990).
[16] R. L. Stratonovich, Sov. Phys. Doklady **2**, 461 (1958).
[17] J. Hubbard, Phys. Rev. Lett. **3**, 77 (1959).
[18] Y. Yamaguchi, J. Barré, F. Bouchet, T. Dauxois, and S. Ruffo, Physica A **337**, 36 (2004).
[19] J. Barré, F. Bouchet, T. Dauxois, S. Ruffo, and Y. Y. Yamaguchi, Physica A **365**, 177 (2006).
[20] P. Hertel and W. Thirring, Ann. Phys. **63**, 520 (1971).
[21] A. H. Monoharan, L. Pandolfo, and J. C. Fyfe, Geophys. Res. Lett. **28**, 1019 (2001).
[22] H. Itoh and M. Kimoto, J. Atmos. Sci. **56**, 2684 (1999).
[23] D. Segré, B. Shenhav, R. Kafri, and D. Lancet, J. Theor. Biol. **213**, 481 (2001).
[24] K. S. Fine, A. C. Cass, W. G. Flynn, and C. F. Driscoll, Phys. Rev. Lett. **75**, 3277 (1995).